




Cite this: *Dalton Trans.*, 2018, **47**, 13949

Elucidating white light emissions in $\text{Tm}^{3+}/\text{Dy}^{3+}$ codoped polyoxometalates: a color tuning and energy transfer mechanism study†

Hechen Wu, Minna Zhi, Vikram Singh, Huafeng Li, Pengtao Ma, * Jingyang Niu 
and Jingping Wang *

The double-tartaric bridging Tm-substituted POM derivative $[\text{N}(\text{CH}_3)_4]_6\text{K}_3\text{H}_7[\text{Tm}(\text{C}_4\text{H}_2\text{O}_6)(\alpha\text{-PW}_{11}\text{O}_{39})]_2 \cdot 27\text{H}_2\text{O}$ (**1**) was successfully synthesized and well characterized by various physico-chemical analyses. Furthermore, the mixed $\text{Dy}^{3+}/\text{Tm}^{3+}$ ion-based POM derivatives $[\text{N}(\text{CH}_3)_4]_6\text{K}_3\text{H}_7[\text{Dy}_x\text{Tm}_{1-x}(\text{C}_4\text{H}_2\text{O}_6)(\alpha\text{-PW}_{11}\text{O}_{39})]_2 \cdot 27\text{H}_2\text{O}$ (**3–8**) were first synthesized and confirmed by PXRD and IR spectra, indicating compounds **3–8** are isomorphic with **1**. The detailed analyses of Ln–O–W bond angle and coordinated aqua ligands around emitting Ln^{3+} ions have revealed that the mentioned negative factors do not effectively affect the luminescence of emitting Ln^{3+} ions in **1–8**. Investigations of PL emissions reveal that **3–8** can display color-tunable PL properties, emitting color from blue to white to yellow. The study of time-resolved emission spectroscopy of **6** indicates the energy can transfer from the LMCT excited state of POM fragments to Tm^{3+} and/or Dy^{3+} ions. Furthermore, the decreased luminescent lifetime of Tm^{3+} ions in **3–8** reasonably verifies the energy transfer from Tm^{3+} to Dy^{3+} ions to efficiently facilitate emissions of the Dy^{3+} centre.

Received 30th June 2018,
Accepted 29th August 2018

DOI: 10.1039/c8dt02671h

rsc.li/dalton

Introduction

Polyoxometalates (POMs) can be viewed as a series of metal-oxo polyhedral building blocks (MO_x), where M is in the highest oxidation state ($\text{M} = \text{V}^{5+}, \text{Nb}^{5+}, \text{Ta}^{5+}, \text{Mo}^{6+}, \text{W}^{6+}$), connected through edge-, corner- or face-sharing fashions.¹ The additional heteroatoms (Si, Ge, P, As, Sb, Se, Te) are mainly introduced into the POM skeleton particularly to stabilize the molecular framework, control structural shape and size, or to alter surface electron density, achieved by compositional variations on the POM skeletons.² The pre-existing investigations indicate that POMs possess various topological structures, redox stability and remarkable electronic properties, which facilitate their role in diverse areas of research, such as catalysis, magnetism, biology, medicine, electro-chemistry and optics, thus helping to solve contemporary challenges related to the environment, energy, health *etc.*³ POMs are an excellent class of inorganic multidentate O-donor ligands that can coor-

dinate to f- and/or d-metal ions, or to organic molecules to form functionalized POM derivatives.⁴

Lanthanide ion (Ln^{3+})-based solid-state luminescent materials are usually applied as phosphors for white light-emitting diode (WLED) applications.⁵ The luminescence of Ln^{3+} ions mainly originates from various f-f electron transitions, which are dominant within their unfilled 4f electronic orbitals and are thus classified as electric-dipole and magnetic-dipole transitions. According to the Judd–Ofelt (JO) theory, these electric-dipole f-f transitions are Laporte forbidden as a result of the same parity 4f electronic configurations ($\Delta L = 0$), which lead to an extremely small absorption coefficient ($\epsilon < 10 \text{ L mol}^{-1} \text{ cm}^{-1}$) and low luminous efficiency.⁶ More importantly, the oxophilic Ln^{3+} ions particularly bind the oxygen donors of the vacant POM anion and thus serve as antenna materials to absorb and transfer energy from the photoexcitation $\text{O} \rightarrow \text{M}$ triplet state to active Ln^{3+} ions *via* ligand to metal charge-transfer (LMCT) transitions within the Ln-POM derivative.⁷

Since the first Ln-POMs were reported in 1971, increasing attention has been placed on the synthesis of such Ln-POMs because of their Lewis acid catalysis and their optical and magnetic properties.⁸ Although plenty of Ln-POMs have been reported, most are restricted to single-component Ln-POM derivatives. Nevertheless, to date, there are few reports on mixed-Ln/Ln' POM-based multifunctional materials.⁹ As we know, white light emission originates from rational combi-

Henan Key Laboratory of Polyoxometalate Chemistry, College of Chemistry and Chemical Engineering, Henan University, Kaifeng, Henan 475004, P. R. China.
E-mail: mpt@henu.edu.cn, jpwang@henu.edu.cn; Fax: (+86) 371-2388 6876

†Electronic supplementary information (ESI) available: Synthesis, TGA, ICP, IR, EDX, STEM maps, the packing arrangement of polyanions, CIE 1931 chromaticity diagram and time-resolved emission spectroscopy. CCDC 1843262. For ESI and crystallographic data in CIF or other electronic format see DOI: 10.1039/c8dt02671h

nations of three primary colors. Different Ln^{3+} ions can emit inherent characteristic Commission International de l'Eclairage (CIE) luminescent color coordinates; thus, the theoretical combination of multiple Ln^{3+} ions can present white light emission properties. To date, some main methods for obtaining white light are the combination of $\text{Tb}^{3+}/\text{Sm}^{3+}$, $\text{Tm}^{3+}/\text{Dy}^{3+}$, $\text{Tb}^{3+}/\text{Eu}^{3+}$, $\text{Tm}^{3+}/\text{Tb}^{3+}/\text{Eu}^{3+}$ or $\text{Yb}^{3+}/\text{Er}^{3+}/\text{Tm}^{3+}$ ions in a single-phase host.¹⁰ In 2012, Wu and coworkers first reported Tb/Eu-POM derivatives, and further study indicates that the chromaticity coordinates for $\text{Tb}_{0.25}\text{Eu}_{0.75}\text{-POM}$ (0.342, 0.362) are close to those of standard white light (0.333, 0.333).^{9a} In addition, Zhou and coworkers reported another two Tb/Eu-POM derivatives in 2017 and 2018.^{9d,g} Therefore, the background discussed offers us a potential opportunity to further explore the design and properties of mixed Ln/Ln'-POM materials.

Herein, the combination of $\text{Tm}^{3+}/\text{Dy}^{3+}$ ions was first chosen to investigate the white light emissions of Ln-POM derivatives. Recently, we successfully obtained a double-tartrate bridging Tm-substituted phosphotungstate $[\text{N}(\text{CH}_3)_4]_6\text{K}_3\text{H}_7[\text{Tm}(\text{C}_4\text{H}_2\text{O}_6)(\alpha\text{-PW}_{11}\text{O}_{39})]_2 \cdot 27\text{H}_2\text{O}$ (**1**) that is isomorphous with the reported $[\text{N}(\text{CH}_3)_4]_6\text{K}_3\text{H}_7[\text{Dy}(\text{C}_4\text{H}_2\text{O}_6)(\alpha\text{-PW}_{11}\text{O}_{39})]_2 \cdot 27\text{H}_2\text{O}$ (**2**).¹¹ Subsequently, a series of $\text{Tm}^{3+}/\text{Dy}^{3+}$ codoped POM derivatives $[\text{N}(\text{CH}_3)_4]_6\text{K}_3\text{H}_7[\text{Tm}_{1-x}\text{Dy}_x(\text{C}_4\text{H}_2\text{O}_6)(\alpha\text{-PW}_{11}\text{O}_{39})]_2 \cdot 27\text{H}_2\text{O}$ (**3–8**) ($x = 0.03\text{--}0.50$) were elaborately synthesized by adjusting the molar ratio of $\text{Tm}^{3+}:\text{Dy}^{3+}$ ions in a similar reaction system. These isomorphous POM derivatives (**3–8**) were fully characterized by elemental analysis, powder X-ray diffraction (PXRD), thermogravimetric analyses (TGA) (Fig. S1†), IR spectra (Fig. S2†), energy dispersive X-ray spectroscopy (EDX) (Fig. S3†), inductively coupled plasma atomic emission spectrometer (ICP-AES; Table S1†) and scanning transmission electron microscopy (STEM) maps. The resulting compounds **3–8** exhibit color-tunable photoluminescence (PL) switching behaviour, *i.e.*, from blue to white and then to yellow. Furthermore, the energy transfer mechanism related to their luminescence was systematically investigated.

Results and discussion

Powder X-ray diffraction

As shown in Fig. 1, the experimental PXRD patterns of **1–8** are in good agreement with the simulated PXRD patterns of **1** that originated from the single-crystal X-ray diffraction structural analyses, indicating that the experimental samples are in good phase purity and $\text{Tm}^{3+}/\text{Dy}^{3+}$ -doped compounds **3–8** are isomorphous with **1**. The difference of intensity between experimental and simulated PXRD patterns are carefully discovered, which may be due to the variation in preferred orientation of the powder sample during the process of collection of the experimental PXRD patterns.

Crystal structure

In this reaction system, the precursor $[\text{P}_2\text{W}_{19}\text{O}_{67}(\text{H}_2\text{O})]^{14-}$ was chosen to construct a series of new Ln-POM derivatives. The

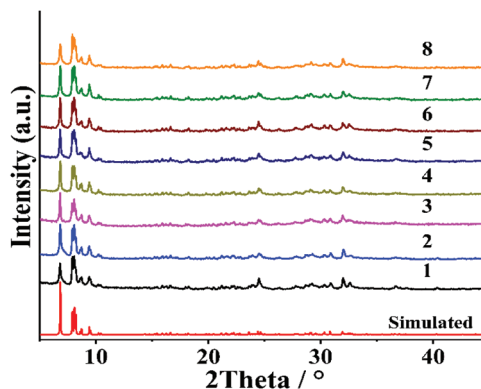


Fig. 1 Simulated single-crystal PXRD of **1** and experimental PXRD patterns of **1–8**.

$\{\text{WO}(\text{H}_2\text{O})\}$ linker can serve as a critical starting point for the dissociation or free rotations of $\{\text{PW}_9\}$ subunits in the reactivity of the precursor $[\text{P}_2\text{W}_{19}\text{O}_{67}(\text{H}_2\text{O})]^{14-}$. In the optimum pH value of 3.2, the reaction of $[\text{P}_2\text{W}_{19}\text{O}_{67}(\text{H}_2\text{O})]^{14-}$ with tartrate ligands and $\text{LnCl}_3 \cdot 6\text{H}_2\text{O}$ in rational molar ratio results in the crystallization of **1–8**. The crystalline nature of these compounds was confirmed by PXRD analyses. All compounds **1–8** are in the same orthorhombic space group $Pna2_1$; hence the structure of **1** is especially described in detail for further comparison with related compounds. Compound **1** contains one dimeric polyanion skeleton $[\text{Tm}(\text{C}_4\text{H}_2\text{O}_6)(\alpha\text{-PW}_{11}\text{O}_{39})]_2^{16-}$, three K^+ ions, six $[\text{N}(\text{CH}_3)_4]^{3+}$ counter cations and twenty-seven lattice water molecules; simultaneously, seven H^+ protons are directly added for charge balance of the negative polyanion. The packing arrangement of polyanions of **1** is shown in Fig. S4.† In the polyanion skeleton of **1**, Tm^{3+} ion occupies the defect site of the $[\alpha\text{-PW}_{11}\text{O}_{39}]^{7-}$ subunit with the $\text{Tm}\text{--}\text{O}\text{--}\text{W}$ bond angles in the range of $134.2(11)$ to $158.7(16)^\circ$ (Fig. 2b and Table S2†). Both the tartrate ligands adopt bridging

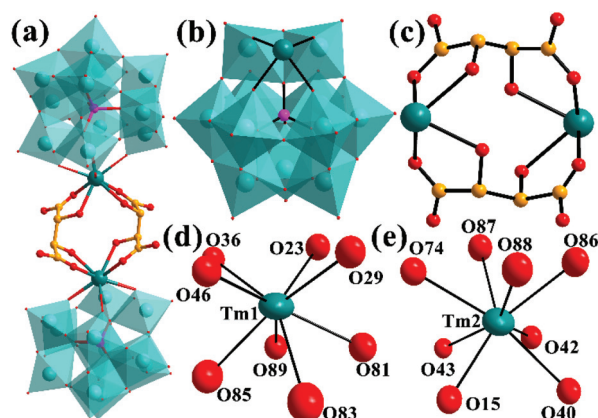


Fig. 2 (a) Polyhedral/ball-and-stick representation of the polyanion in **1**; (b) polyhedral/ball-and-stick representation of $[\text{TmPW}_{11}\text{O}_{39}]^{4-}$ units; (c) the coordination mode of tartrate ligands; the coordination environment of (d) Tm1 and (e) Tm2 centres (color code: WO_6 , aqua; W, aqua; P, pink; Tm, teal; O, red; C, light orange).

coordination modes linking two Keggin-type $[\text{TmPW}_{11}\text{O}_{39}]^{4-}$ units through Tm–O covalent bonds to form the dimeric polyanion in **1** (Fig. 2a and c). More specifically, the Tm1 atom is 8-fold coordinated by four O atoms (O23, O29, O36 and O46) of the $[\alpha\text{-PW}_{11}\text{O}_{39}]^{7-}$ subunit, and another four O atoms (O81, O83, O85 and O89) from two tartrate ligands with Tm1–O bond lengths and O–Tm1–O bond angles of 2.26(3)–2.48(3) Å and of 68.8(12)–146.9(12)° respectively (Fig. 2d, Tables S2 and S3†). By comparison, Tm2 atom is surrounded by four O15, O40, O42 and O43 atoms (from $[\alpha\text{-PW}_{11}\text{O}_{39}]^{7-}$ group) and O74, O86, O87 and O88 atoms (from two tartrate ligands) with Tm2–O bond lengths of 2.25(2)–2.43(3) Å and O–Tm2–O bond angles of 60.1(13)–147.3(11)° (Fig. 2e, Tables S2 and S3†).

STEM-EDX study

The STEM-EDX element maps in Fig. 3, S5 and S6† are presented for **6** as a representative of $\text{Tm}^{3+}/\text{Dy}^{3+}$ -POMs; they indicate a uniform distribution of C, N, O, P, K, Dy, Tm and W throughout the crystalline structure.

The EDX spectra for **1–8**, shown in Fig. S3,† suggest the composition of Tm^{3+} and Dy^{3+} ions could be systematically tuned across the entire $\text{Tm}^{3+}/\text{Dy}^{3+}$ -POMs. The composition of Tm^{3+} and Dy^{3+} ions in $\text{Tm}^{3+}/\text{Dy}^{3+}$ -POMs can be modulated by varying the Ln^{3+} chloride reagent stoichiometries during the synthesis, and all synthesized samples contain similar total Ln^{3+} ions (Tm^{3+} and/or Dy^{3+}).

PL properties

The luminescence of Ln-based complexes is limited due to the lower molar absorption coefficients; hence, the POM compositions, upon photoexcitation, could act as antenna ligands to sensitize the emission of Tm^{3+} or Dy^{3+} ions in **1** and **2**. The PL emission and excitation spectra of **1** and **2** were investigated at room temperature (Fig. S7 and S8†). Under excitation at 360 nm, the emission spectrum of **1** displays a strong emission signal at 452 nm and a weaker emission at 481 nm, which could be attributed to the $^1\text{D}_2 \rightarrow ^3\text{F}_4$ and $^1\text{G}_4 \rightarrow ^3\text{H}_6$ characteristic f–f transitions of Tm^{3+} ion, respectively (Fig. S7a†). Weak emissions at 410 nm and 423 nm, other than the f–f tran-

sitions of Tm^{3+} ion, should be assigned to $^3\text{T}_{1u} \rightarrow ^1\text{A}_{1g}$ transitions of POM fragments in **1**. To further verify our hypothesis, the emission spectrum of $[\text{P}_2\text{W}_{19}\text{O}_{67}(\text{H}_2\text{O})]^{14-}$ precursor was measured under the same conditions (Fig. S9†). Characteristic emissions of Dy^{3+} ion upon excitation at 367 nm can be detected at 480 nm ($^4\text{F}_{9/2} \rightarrow ^6\text{H}_{15/2}$), 573 nm ($^4\text{F}_{9/2} \rightarrow ^6\text{H}_{13/2}$) and 663 nm ($^4\text{F}_{9/2} \rightarrow ^6\text{H}_{11/2}$) (Fig. S7b†). The emission intensity at 573 nm is much higher than at 480 and 663 nm, possibly due to the $^4\text{F}_{9/2} \rightarrow ^6\text{H}_{15/2}$ electric dipole f–f transitions, which are stronger by several orders of magnitude of magnetic dipole transition. Previous works by Yamase,^{7a} Boskovic,^{8c} and Reinoso¹² have shown that the approximate bond angle of 150° between Ln–O–W bond can quench the luminescence of Ln^{3+} ion on account of effective d^1 electrons hopping through electron delocalization and $f\pi$ – $p\pi$ – $d\pi$ orbital mixing. In addition, the coordination of aqua and similar molecules may cause non-radiative quenching of Ln^{3+} ion luminescence due to the coupling with high O–H oscillators. In the presence of eight such Tm–O–W bonds, the bond angles can be divided into two categories in **1**. In detail, the Tm–O_x–W (O_x = O15, O23, O36, O40) bond angles in the range of 134.2(11)–142.7(18)° cannot efficiently facilitate the luminescence quenching, and Tm–O_y–W (O_y = O29, O42, O43, O46) bond angles of 154.9(18)–158.7(16)° may affect but not efficiently quench the emissions of Tm^{3+} . Obviously, the eight coordinated O atoms around each Tm emitting centre are the four O atoms from POM fragments and four O atoms from two tartrate ligands; hence, there is no high O–H frequency oscillator impairing the emission of Tm^{3+} ions in **1**. For structurally isomorphous compounds **2–8**, the structure has similar characteristics as those in **1**, and thus the influences on luminescence properties caused by Ln–O–W bond $f\pi$ – $p\pi$ – $d\pi$ orbital mixing and coordinated aqua ligands are quite similar to those for **1**. Therefore, this double-tartronic bridging Ln^{3+} -substituted POM derivatives were chosen for further exploring the white light-emitting characteristics.

Fig. S10† and Table 1 depict the corresponding CIE chromaticity coordinates, color purity, CCT and emission colors of **1** and **2**. Compound **1** is located on the blue area (0.144, 0.178) in the CIE 1931 chromaticity diagram, and color purity is 77.89%. Interestingly, compound **2** appears at a yellow area (0.384, 0.431), and color purity and CCT are 44.46% and 4226 K, respectively.

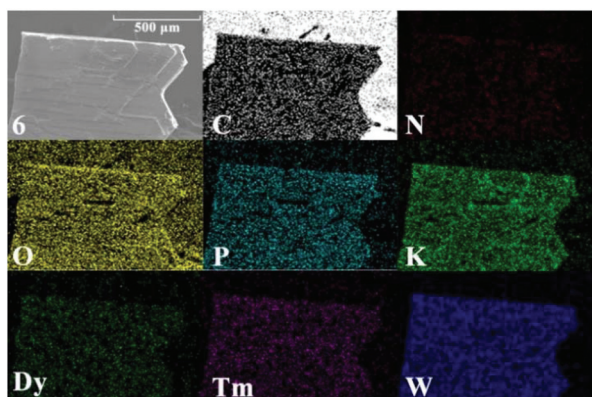


Fig. 3 STEM-EDX element maps of **6**.

Table 1 CIE chromaticity coordinates, color purity, CCT and emitting color of **1–8**

Samples	(x, y)	Color purity (%)	CCT (K)	Emission color
1	0.144, 0.178	77.89		Blue
2	0.384, 0.431	44.46	4226	Yellow
3	0.256, 0.267	32.07	15 453	Blue
4	0.295, 0.310	14.87	7884	Blue-white
5	0.310, 0.334	7.85	6612	White
6	0.325, 0.349	3.15	5817	White
7	0.336, 0.365	10.40	5366	Yellow-white
8	0.358, 0.400	27.53	4740	Yellow

Color-tunable PL properties

The study of $\text{Tm}^{3+}/\text{Dy}^{3+}$ -doped materials, such as $\text{YAl}_3(\text{BO}_3)_4$: $\text{Tm}^{3+}/\text{Dy}^{3+}$, $\text{Ca}_9\text{Y}(\text{PO}_4)_7$: $\text{Tm}^{3+}/\text{Dy}^{3+}$ and $\text{MgIn}_2\text{P}_4\text{O}_{14}$: $\text{Tm}^{3+}/\text{Dy}^{3+}$ phosphors, have shown that they can display preferable tunable luminescence color.¹³ As shown in Fig. S10† and Table 1, the CIE luminescent color coordinates of **1** and **2** are blue and yellow, and the connection line between the points of **1** and **2** in the chromaticity diagram appears in the white light area. Theoretically, the appropriate proportion of Tm^{3+} and Dy^{3+} ions can generate white light. The white-light-emitting POM derivatives have been mentioned by Wu^{9a} and Zhou^{9d,g} with the tunable behaviour of Tb^{3+} and Eu^{3+} ions. The chromaticity coordinates of the reported Tb/Eu -POM in white are not tightly close to the standard white light point (0.333, 0.333), and the aqua molecules coordinated to the $\text{Tb}^{3+}/\text{Eu}^{3+}$ centres may impair the emission of $\text{Tb}^{3+}/\text{Eu}^{3+}$ ions.^{9a,d} Herein, we first choose double-tartaric bridging $\text{Tm}^{3+}/\text{Dy}^{3+}$ -doped POM derivatives, and no aqua molecules take part in the coordination of $\text{Tm}^{3+}/\text{Dy}^{3+}$ centres.

Fig. 4 depicts the emission spectra of **3–8** under excitation at 360 nm and the corresponding CIE chromaticity diagram. Six peaks at 410, 423, 452, 480, 573 and 663 nm can be observed, indicating the existence of Tm^{3+} and Dy^{3+} ions in **3–8** (Fig. 4a).

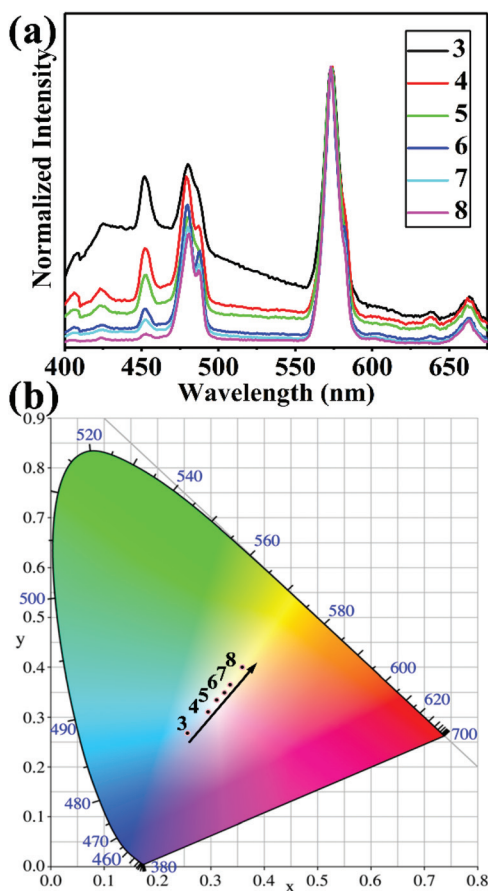


Fig. 4 (a) PL emission spectra of **3–8** ($\lambda_{\text{ex}} = 360$ nm); (b) the CIE chromaticity diagram of **3–8**.

It should be noted that the emission of ${}^4\text{F}_{9/2} \rightarrow {}^6\text{H}_{15/2}$ transition (480 nm) of the Dy^{3+} ion obviously overlaps the ${}^1\text{G}_4 \rightarrow {}^3\text{H}_6$ transition (481 nm) of Tm^{3+} ion in the layout. From Fig. 4b and Table 1, it can be seen that the CIE color coordinates of **3** locates in the blue area. As the proportion of doped Dy^{3+} ion increases, the normalized emission intensity at 410, 423, 452 and 480 nm gradually decreases and the CIE color coordinates of **3–8** synchronously vary from blue to white to yellow, in good agreement with the previous observation on such reports. Especially, the chromaticity coordinates of **6** (0.325, 0.349) locate near the standard white light point (0.333, 0.333). The correlated color temperature (CCT) decreases from the 15 453 K (cool color) of **3** to the 4740 K (warm color) of **8** with the increase of Dy^{3+} ion concentration. The cool white (CW) light emitting CCT at 5817 K of **6** also can meet several standards of lighting materials.

Energy transfer mechanism

The energy transfer process and mechanism from POM to Ln^{3+} ion has been previously documented.⁷ The POM fragments can be excited from ${}^1\text{A}_{1g}$ level to triplet state under irradiation and subsequently transfer energy to the Ln^{3+} ion to sensitize the emitting Ln^{3+} centres *via* antenna effect. Fig. 5 shows the comparison of excitation and emission spectra of **1** and **2**. Noticeably, the partial overlap at around 360 nm between the excitation spectrum of **1** (Fig. 5a) and excitation spectrum of **2** (Fig. 5c) means that the emissions of **1** and **2** can be excited by an identical excitation of 360 nm. Furthermore, the obvious overlap at 452 nm between the emission spectrum of **1** (${}^1\text{D}_2 \rightarrow {}^3\text{F}_4$) (Fig. 5b) and excitation spectrum of **2** (${}^6\text{H}_{15/2} \rightarrow {}^4\text{H}_{11/2}$) (Fig. 5c) implies that the energy can theoretically transfer from Tm^{3+} to Dy^{3+} in **3–8**. Time resolved emission spectroscopy was conducted to investigate the energy transfer process (Fig. 6a, S11 and S12†). As shown in Fig. 6a, the emission at 410 nm appears first, and the intensity reaches the maximum at 39.00 μs . Soon afterwards, the emission at 423 nm initially emerges at 39.75 μs

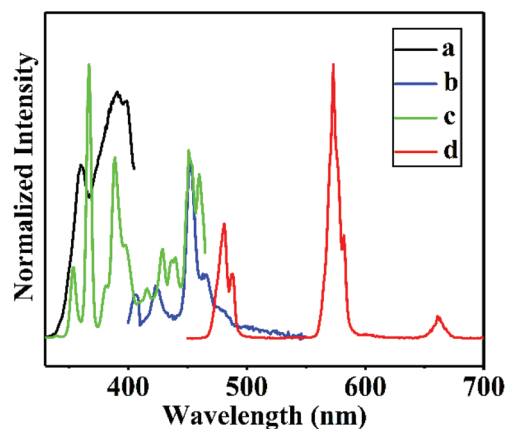


Fig. 5 The comparison of both PL excitation and PL emission spectra of **1** and **2**. Black line (a) excitation spectrum of **1**, blue line (b) emission spectrum of **1**, green line (c) excitation spectrum of **2**, red line (d) emission spectrum of **2**.

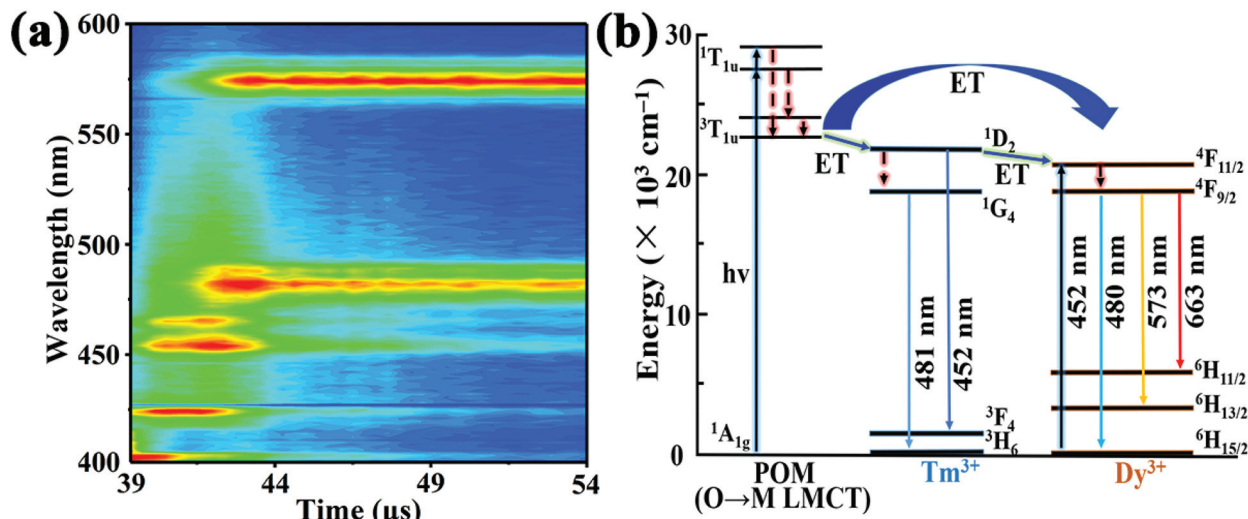


Fig. 6 (a) The time resolved emission spectroscopy of **6** ($\lambda_{\text{ex}} = 360$ nm). Color changing from blue to green to yellow to red represents an increase in emission intensity; (b) schematic energy level diagram and energy transfer (ET) process in **6**.

and reaches the maximum at 40.15 μs . Meanwhile, the characteristic emission of Tm^{3+} at 452 nm and the characteristic emissions of Dy^{3+} at 480 and 573 nm appear at 39.95, 41.55 and 42.00 μs , respectively. This phenomenon signifies the energy transfer process from POM to Tm^{3+} and/or Dy^{3+} ions, which appears in **6**. The reason for the emissions of Dy^{3+} ion being next to that of Tm^{3+} ion may be the superior match of the ${}^3\text{T}_{1\text{u}}$ triplet state of excited POM fragments to the ${}^1\text{D}_2$ excited level of Tm^{3+} ion, compared with the ${}^4\text{F}_{11/2}$ excited level of Dy^{3+} ion.

In addition, the intensity of emission at 480 nm decreases after the quenching of the characteristic emission intensity of Tm^{3+} ion at 452 nm, strongly demonstrating that energy transfer occurs from Tm^{3+} to Dy^{3+} ions (Fig. 6b). To prove the possible mechanism, the luminescence lifetime measurements, as an important tool for demonstrating energy transfer between Ln and Ln' centres,¹⁴ at 452 nm of the Tm^{3+} emitting centres in **1** and **3–8** were monitored upon excitation at 360 nm and emission at 452 nm. The lifetime of **1** and **3–8** adhere to a double exponential decay mode (Fig. S13[†]), and the average lifetime τ^* could be generally regarded as the experimental lifetime value. As shown in Fig. S13 and Table 2, the lifetime for a Tm^{3+} emitting centre decreases in **3–8** compared with

Table 2 Biexponential fitting results of Tm^{3+} emitting centres in **1** and **3–8** upon excitation at 360 nm and emission at 452 nm

Sample	τ_1 (μs)	α_1 (%)	τ_2 (μs)	α_2 (%)	τ^* (μs)
1	2.18	24.37	11.14	75.63	10.61
3	2.03	22.81	10.17	77.19	9.72
4	1.98	22.99	10.05	77.01	9.60
5	1.97	22.78	9.82	77.22	9.38
6	1.83	25.46	10.09	74.54	9.61
7	1.73	25.89	10.09	74.11	9.62
8	1.67	21.56	10.04	78.44	9.67

Table 3 The calculated energy gap of different transitions of states

Transitions of states	Wavelength (nm)	Energy gap ($\times 10^3 \text{ cm}^{-1}$)
	360	27.78
${}^1\text{D}_2 \rightarrow {}^3\text{F}_4$	452	22.12
${}^6\text{H}_{15/2} \rightarrow {}^4\text{H}_{11/2}$	452	22.12
${}^1\text{G}_4 \rightarrow {}^3\text{H}_6$	481	20.79
${}^4\text{F}_{9/2} \rightarrow {}^6\text{H}_{15/2}$	480	20.83
${}^4\text{F}_{9/2} \rightarrow {}^6\text{H}_{13/2}$	573	17.45
${}^4\text{F}_{9/2} \rightarrow {}^6\text{H}_{11/2}$	663	15.08

that in **1**. The phenomenon also reasonably proved the energy transfer from Tm^{3+} to Dy^{3+} ions in these $\text{Tm}^{3+}/\text{Dy}^{3+}$ -doped POMs. The changes in PL lifetime are well consistent with the time resolved emission spectroscopy and the pre-suppositions. Furthermore, several theoretical energy gaps have been calculated and are summarized in Table 3 to verify this energy transfer mechanism. It can be found that the ${}^1\text{D}_2 \rightarrow {}^3\text{F}_4$ and ${}^6\text{H}_{15/2} \rightarrow {}^4\text{H}_{11/2}$ transitions have the same energy gap ($22.12 \times 10^3 \text{ cm}^{-1}$), and the well-matched energy gaps reasonably support that energy transfer may occur from Tm^{3+} to Dy^{3+} ions.

Conclusions

In summary, a series of single-component and mixed $\text{Tm}^{3+}/\text{Dy}^{3+}$ -doped POM derivatives (**1–8**) were successfully synthesized and characterized by IR spectra, elemental analysis, PXRD, TGA, ICP and EDX. The structural analyses indicate Ln–O–W bond $\text{f}\pi\text{--p}\pi\text{--d}\pi$ orbital mixing may, to some extent, affect the luminescence emissions of Ln³⁺ emitting centres in **1–8**. The investigations of color-tunable PL emission revealed that the CIE luminescent color coordinates of **3–8** can be tuned from blue to white to yellow by increasing the doping pro-

portion of Dy³⁺ ion. Particularly, the CIE 1931 chromaticity coordinates of **6** (0.325, 0.349) are in close proximity to the standard white light point (0.333, 0.333). Time resolved emission spectroscopy was conducted to confirm the energy transfer from the LMCT excited state of POM to Tm³⁺ and Dy³⁺ ions. The changes in the luminescence lifetime of Tm³⁺ emitting centre in **1** and **3–8** reasonably support the hypothesis that efficient energy transfer exists between Tm³⁺ and Dy³⁺ ions.

Experimental section

Material and physical measurements

All chemicals were commercially obtained and used as received. The lacunary precursor K₁₄[P₂W₁₉O₆₉(H₂O)]·24H₂O was synthesized according to the reported literature and confirmed by IR spectrum.¹⁵ Elemental analyses (C, H and N) were measured on an Elementar Vario EL cube CHNS analyser. PXRD data were recorded using an X-ray powder diffractometer (Bruker, D8 Advance) equipped with Cu K α radiation (λ = 1.5418 Å). IR spectra were measured using KBr pellets on a Bruker VERTEX-70 spectrometer in the range of 400–4000 cm⁻¹. Scanning transmission electron microscopy (STEM) images and energy dispersive X-ray spectroscopy (EDX) measurements were recorded on a JSM-7610F scanning electron microscope with an OXFORD x-act EDS system. Analyses for Tm and Dy atoms were conducted on a PerkinElmer Optima 2000 ICP-OES spectrometer. TGA was performed in flowing N₂ from 25 °C to 800 °C at a heating rate of 10 °C min⁻¹ on a NETZSCH STA 449 F5 Jupiter thermal analyser. PL emission spectra, PL excitation spectra, PL decay time curves and time resolved emission spectroscopy were measured on an Edinburgh FLS 980 fluorescence spectrophotometer equipped with a monochromated 450 W Xe-arc excitation source. The Commission Internationale de L'Eclairage (CIE) 1931 chromaticity coordinates, color purity and CCT were calculated according to the international CIE standards.

Synthesis of 1–8

Synthesis of 1: TmCl₃·6H₂O (0.228 g, 0.595 mmol) was dissolved in 30 mL of deionized water, and then tartaric acid (0.120 g, 0.800 mmol) and precursor K₁₄[P₂W₁₉O₆₉(H₂O)]·24H₂O (2.120 g, 0.465 mmol) were added step by step with stirring. The pH value of the mixture was adjusted to approximately 3.2 by 3 M KOH solution and heated to 60 °C for 1.5 h. Subsequently, tetra methyl ammonium chloride (TMACl) (0.110 g, 1.000 mmol) was added and stirred for another 30 min. The resulting solution was cooled to room temperature and filtered to evaporate for two weeks at room temperature to gain suitable crystals for X-ray structure determination. Yield: 22.9% (0.480 g, based on TmCl₃·6H₂O [0.228 g, 0.595 mmol]). IR (KBr, cm⁻¹) (Fig. S2†): 3450 (br), 3038 (w), 1619 (s), 1486 (s), 1098 (s), 1050 (s), 952 (s), 890 (s), 825 (s) and 720 (w). Elemental analyses (%): calcd, C, 5.46; H, 1.96; N, 1.19; found, C, 5.51; H, 1.85; N, 1.23. **Synthesis of 2–8:** The synthesis of Tm_xDy_{1-x}-POM is similar to Tm-POM except

TmCl₃·6H₂O was replaced by the mixture of DyCl₃·6H₂O and TmCl₃·6H₂O in rational proportions (see the ESI†). **2:** IR (KBr, cm⁻¹): 3445 (br), 3043 (w), 1622 (s), 1485 (s), 1095 (s), 1050 (s), 949 (s), 890 (s), 825 (s) and 715 (w). Elemental analyses (%): calcd, C, 5.47; H, 1.97; N, 1.20; found, C, 5.49; H, 1.69; N, 1.23. **3:** IR (KBr, cm⁻¹): 3448 (br), 3041 (w), 1620 (s), 1486 (s), 1095 (s), 1048 (s), 948 (s), 890 (s), 830 (s) and 727 (w). Elemental analyses (%): calcd, C, 5.46; H, 1.99; N, 1.19; found, C, 5.52; H, 1.84; N, 1.34. **4:** IR (KBr, cm⁻¹): 3450 (br), 3038 (w), 1623 (s), 1485 (s), 1094 (s), 1049 (s), 950 (s), 889 (s), 832 (s) and 725 (w). Elemental analyses (%): calcd, C, 5.47; H, 1.99; N, 1.20; found, C, 5.51; H, 1.87; N, 1.29. **5:** IR (KBr, cm⁻¹): 3449 (br), 3041 (w), 1620 (s), 1484 (s), 1100 (s), 1049 (s), 955 (s), 892 (s), 829 (s) and 725 (w). Elemental analyses (%): calcd, C, 5.47; H, 1.99; N, 1.20; found, C, 5.50; H, 1.89; N, 1.28. **6:** IR (KBr, cm⁻¹): 3452 (br), 3039 (w), 1621 (s), 1486 (s), 1095 (s), 1050 (s), 949 (s), 889 (s), 830 (s) and 725 (w). Elemental analyses (%): calcd, C, 5.48; H, 2.00; N, 1.20; found, C, 5.53; H, 1.80; N, 1.32. **7:** IR (KBr, cm⁻¹): 3452 (br), 3038 (w), 1620 (s), 1486 (s), 1100 (s), 1050 (s), 948 (s), 895 (s), 830 (s) and 725 (w). Elemental analyses (%): calcd, C, 5.49; H, 2.00; N, 1.20; found, C, 5.53; H, 1.86; N, 1.35. **8:** IR (KBr, cm⁻¹): 3450 (br), 3039 (w), 1622 (s), 1486 (s), 1099 (s), 1053 (s), 948 (s), 890 (s), 832 (s) and 724 (w). Elemental analyses (%): calcd, C, 5.52; H, 2.01; N, 1.21; found, C, 5.56; H, 1.68; N, 1.28.

X-ray crystallography

A suitable sample of **1** was recorded on a Bruker Apex II CCD diffractometer for the crystallographic study at 296(2) K, with graphite-monochromated Mo K α radiation (λ = 0.71073 Å). Intensity data were corrected for Lorentz and polarization effects as well as for multi-scan absorption. The structure was detected by direct methods, and heavy atoms were located by full-matrix least-squares refinements on F^2 and Fourier syntheses using the SHELXTL-97 program package, which was further refined by full-matrix least squares on F^2 using the SHELXL-2018/1 program package.¹⁶ The SQUEEZE program was used to remove the contributions of all the solvent water and disordered material.¹⁷ In the final refinement cycles, all the atoms, including heavy atoms P, W, and Tm and light atoms O, N, and C (except for O78, C10, C24 and C25 atoms) were refined anisotropically. The command 'omit-3 50.2' was used to omit the weak reflection above 50 degrees. The command 'ISOR' and 'SIMU' were used to restrain the non-H atoms with ADP and NPD problems, which lead to a relatively high restraint value. The TMA groups were restrained to keep the regular tetrahedral geometry by DFIX and SADI commands. The ADP or NDP alerts of two P atoms and numerous C, N, O atoms were resolved by ISOR command. The command 'DELU' was used to solve the large Hirshfeld difference of the anisotropic displacement parameters along the chemical bonds of W12–O63, W16–O54, C8–O90, C5–C6, and O76–C1. However, none of these deficiencies affect the structural details and reliability of the polyanion structure. The hydrogen atoms of the tartaric groups were placed in calculated positions and then refined using a riding model. Three

Table 4 Crystallographic data and structure refinement for **1**

1	
Empirical formula	C ₃₂ H ₁₁₇ K ₃ N ₆ O ₁₁₇ P ₂ W ₂₂ Tm ₂
Formula weight	7019.83
Temperature/K	296(2)
Crystal system	Orthorhombic
Space group	<i>Pna</i> 2 ₁
<i>a</i> [Å]	22.095 (2)
<i>b</i> [Å]	13.0551 (13)
<i>c</i> [Å]	52.019 (5)
α [°]	90
β [°]	90
γ [°]	90
<i>V</i> [Å ³]	15 005 (3)
<i>Z</i>	4
ρ_{calcd} [g cm ⁻³]	2.846
μ [mm ⁻¹]	18.055
<i>F</i> (000)	11 304.0
Index ranges	−26 ≤ <i>h</i> ≤ 26 −13 ≤ <i>k</i> ≤ 15 −45 ≤ <i>l</i> ≤ 62
Reflections collected	73 435
Independent reflections	21 850 [<i>R</i> _{int} = 0.0963]
data/restraints/parameters	21 850/745/1364
Goodness-of-fit on <i>F</i> ²	1.052
<i>R</i> ₁ , <i>wR</i> ₂ [<i>I</i> > 2σ(<i>I</i>)]	0.0623, 0.1454
Largest diff. peak/hole/e Å ⁻³	3.34/−3.17

disordered K⁺ ions were determined by EDX measurement results. The SQUEEZE program performed in OLEX was further used to calculate and evaluate the possible numbers of the solvent water molecules in the four accessible voids of the crystal structure. A total of 66 solvent water molecules should be added to the chemical formula [N(CH₃)₄]₆K₃H₇[Tm(C₄H₂O₆)] (α-PW₁₁O₃₉)₂·66H₂O on the basis of the calculation results. However, the TGA and CHN elemental analysis results showed that the number of water molecules might be 27 for the empirical formula [N(CH₃)₄]₆K₃H₇[Tm(C₄H₂O₆)] (α-PW₁₁O₃₉)₂·27H₂O. This might be attributed to the weathering of crystals of **1**. Gradually, most of the highly disordered water molecules are lost in the process of drying and storing at room temperature.¹⁸ The crystal data and structure refinement parameters are listed in Table 4.

Conflicts of interest

There are no conflicts to declare.

Acknowledgements

This work was financially supported by the National Nature Science Foundation of China (21771053, 21771054, 21571050, 21573056), Natural Science Foundation of Henan Province (132300410144 and 162300410015), Henan Province science and technology attack plan project (182102210237) and the 2018 Students Innovative Pilot Plan of Henan University (201810475016).

Notes and references

- (a) Q. Zheng, L. Vilà-Nadal, Z. Lang, J.-J. Chen, D.-L. Long, J. S. Mathieson, J. M. Poblet and L. Cronin, *J. Am. Chem. Soc.*, 2018, **140**, 2595–2601; (b) P. Ma, F. Hu, J. Wang and J. Niu, *Coord. Chem. Rev.*, 2018, DOI: 10.1016/j.ccr.2018.02.010; (c) M. Raula, G. GanOr, M. Saganovich, O. Zeiri, Y. Wang, M. R. Chierotti, R. Gobetto and I. A. Weinstock, *Angew. Chem., Int. Ed.*, 2015, **54**, 12416–12421; (d) Y. P. Jeannin, *Chem. Rev.*, 1998, **98**, 51–76.
- (a) H. N. Miras, J. Yan, D.-L. Long and L. Cronin, *Chem. Soc. Rev.*, 2012, **41**, 7403; (b) D. L. Long, R. Tsunashima and L. Cronin, *Angew. Chem., Int. Ed.*, 2010, **49**, 1736–1758; (c) D.-L. Long, E. Burkholder and L. Cronin, *Chem. Soc. Rev.*, 2007, **36**, 105–121; (d) J.-C. Liu, Q. Han, L.-J. Chen, J.-W. Zhao, C. Streb and Y.-F. Song, *Angew. Chem., Int. Ed.*, 2018, **57**, 8416–8420; (e) K. Stroobants, E. Moelants, H. G. T. Ly, P. Proost, K. Bartik and T. N. Parac-Vogt, *Chem. – Eur. J.*, 2013, **19**, 2848–2858.
- (a) J. M. Clemente-Juan, E. Coronado and A. Gaita-Ariño, *Chem. Soc. Rev.*, 2012, **41**, 7464; (b) H. Lv, Y. V. Geletii, C. Zhao, J. W. Vickers, G. Zhu, Z. Luo, J. Song, T. Lian, D. G. Musaev and C. L. Hill, *Chem. Soc. Rev.*, 2012, **41**, 7572; (c) J. T. Rhule, C. L. Hill and D. A. Judd, *Chem. Rev.*, 1998, **98**, 327–357; (d) D. E. Katsoulis, *Chem. Rev.*, 1998, **98**, 359–387; (e) S. Chen, P. Ma, H. Luo, Y. Wang, J. Niu and J. Wang, *Chem. Commun.*, 2017, **53**, 3709–3712; (f) L. Vilà-Nadal and L. Cronin, *Nat. Rev. Mater.*, 2017, **2**, 17054; (g) L. Vandebroek, E. De Zitter, H. G. T. Ly, D. Conić, T. Mihaylov, A. Sap, P. Proost, K. Pierloot, L. Van Meervelt and T. N. Parac-Vogt, *Chem. – Eur. J.*, 2018, **24**, 10099–10108; (h) T. Quanten, P. Shestakova, D. Van Den Bulck, C. Kirschhock and T. N. Parac-Vogt, *Chem. – Eur. J.*, 2016, **22**, 3775–3784.
- (a) P. Gouzerh and A. Proust, *Chem. Rev.*, 1998, **98**, 77–111; (b) A. Proust, B. Matt, R. Villanneau, G. Guillemot, P. Gouzerh and G. Izzet, *Chem. Soc. Rev.*, 2012, **41**, 7605; (c) J.-W. Zhao, Y.-Z. Li, L.-J. Chen and G.-Y. Yang, *Chem. Commun.*, 2016, **52**, 4418–4445; (d) X. Ma, H. Li, L. Chen and J. Zhao, *Dalton Trans.*, 2016, **45**, 4935–4960.
- (a) C. C. Lin, Y.-T. Tsai, H. E. Johnston, M.-H. Fang, F. Yu, W. Zhou, P. Whitfield, Y. Li, J. Wang, R.-S. Liu and J. P. Attfield, *J. Am. Chem. Soc.*, 2017, **139**, 11766–11770; (b) X. Chen, P. Dai, X. Zhang, C. Li, S. Lu, X. Wang, Y. Jia and Y. Liu, *Inorg. Chem.*, 2014, **53**, 3441–3448; (c) B. Zhang, J.-W. Wang, L.-Y. Hao, X. Xu, S. Agathopoulos, L.-J. Yin, C.-M. Wang and H. T. Hintzen, *J. Am. Ceram. Soc.*, 2017, **100**, 257–264; (d) M. R. Krames, O. B. Shchekin, R. Mueller-Mach, G. O. Mueller, Z. Ling, G. Harbers and M. G. Craford, *J. Disp. Technol.*, 2007, **3**, 160; (e) W. Liu, Y. Fang, G. Z. Wei, S. J. Teat, K. Xiong, Z. Hu, W. P. Lustig and J. Li, *J. Am. Chem. Soc.*, 2015, **137**, 9400–9408; (f) W.-T. Chen, H.-S. Sheu, R.-S. Liu and J. P. Attfield, *J. Am. Chem. Soc.*, 2012, **134**, 8022–8025.
- (a) *Rare earth coordination chemistry: fundamentals and applications*, ed. C.-H. Huang, John Wiley & Sons, 2010,

- p. 6; (b) B. R. Judd, *Phys. Rev.*, 1962, **127**, 750; (c) G. S. Ofelt, *J. Chem. Phys.*, 1962, **37**, 511; (d) D. William, J. Horrocks and R. S. Daniel, *J. Am. Chem. Soc.*, 1979, **101**, 334–340.
- 7 (a) T. Yamase, *Chem. Rev.*, 1998, **98**, 307–325; (b) H. Wu, R. Wan, Y. Si, P. Ma, J. Wang and J. Niu, *Dalton Trans.*, 2018, **47**, 1958–1965; (c) P. Ma, F. Hu, Y. Huo, D. Zhang, J. Niu and J. Wang, *Cryst. Growth Des.*, 2017, **17**, 1947–1956; (d) T. Yamase, T. Kobayashi, M. Sugeta and H. Naruke, *J. Phys. Chem. A*, 1997, **101**, 5046–5053; (e) S. Zhang, K. Wang, D. Zhang, P. Ma, J. Niu and J. Wang, *CrystEngComm*, 2012, **14**, 8677; (f) S. Zhang, J. Zhao, P. Ma, H. Chen, J. Niu and J. Wang, *Cryst. Growth Des.*, 2012, **12**, 1263–1272; (g) H. Li, Y. Liu, R. Zheng, L. Chen, J.-W. Zhao and G.-Y. Yang, *Inorg. Chem.*, 2016, **55**, 3881–3893; (h) Y. Liu, H. Li, C. Lu, P. Gong, X. Ma, L. Chen and J. Zhao, *Cryst. Growth Des.*, 2017, **17**, 3917–3928; (i) H.-L. Li, Y.-J. Liu, J.-L. Liu, L.-J. Chen, J.-W. Zhao and G.-Y. Yang, *Chem. – Eur. J.*, 2017, **23**, 2673–2689.
- 8 (a) R. D. Peacock and T. J. R. Weakley, *J. Chem. Soc. A*, 1971, 1836–1839; (b) L. Jin, X.-X. Li, Y.-J. Qi, P.-P. Niu and S.-T. Zheng, *Angew. Chem., Int. Ed.*, 2016, **55**, 13793–13797; (c) C. Ritchie, E. G. Moore, M. Speldrich, P. Kögerler and C. Boskovic, *Angew. Chem., Int. Ed.*, 2010, **49**, 7702–7705; (d) J. Wang, Y. Niu, M. Zhang, P. Ma, C. Zhang, J. Niu and J. Wang, *Inorg. Chem.*, 2018, **57**, 1796–1805; (e) R. Ban, X. Sun, J. Wang, P. Ma, C. Zhang, J. Niu and J. Wang, *Dalton Trans.*, 2017, **46**, 5856–5863; (f) P. Ma, R. Wan, Y. Si, F. Hu, Y. Wang, J. Niu and J. Wang, *Dalton Trans.*, 2015, **44**, 11514–11523; (g) S. Zhang, Y. Wang, J. Zhao, P. Ma, J. Wang and J. Niu, *Dalton Trans.*, 2012, **41**, 3764; (h) X. Wang, Y. Liu, M. Jin, Y. Wu, L. Chen and J.-W. Zhao, *Cryst. Growth Des.*, 2017, **17**, 5295–5308; (i) K. Wang, D. Zhang, J. Ma, P. Ma, J. Niu and J. Wang, *CrystEngComm*, 2012, **14**, 3205–3212; (j) P. Ma, R. Wan, Y. Wang, F. Hu, D. Zhang, J. Niu and J. Wang, *Inorg. Chem.*, 2016, **55**, 918–924.
- 9 (a) W. Zhao, C. Zou, L. Shi, J. Yu, G. Qian and C. Wu, *Dalton Trans.*, 2012, **41**, 10091–10096; (b) R. Sato, K. Suzuki, M. Sugawa and N. Mizuno, *Chem. – Eur. J.*, 2013, **19**, 12982–12990; (c) M. Shiddiq, D. Komijani, Y. Duan, A. Gaita-Ariño, E. Coronado and S. Hill, *Nature*, 2016, **531**, 348–351; (d) H. Ji, X. Li, D. Xu, Y. Zhou, L. Zhang, Z. Zuhra and S. Yang, *Inorg. Chem.*, 2017, **56**, 156–166; (e) A. M. Kaczmarek, K. Van Hecke and R. Van Deun, *Inorg. Chem.*, 2017, **56**, 3190–3200; (f) A. M. Kaczmarek, J. Liu, B. Laforce, L. Vincze, K. Van Hecke and R. Van Deun, *Dalton Trans.*, 2017, **46**, 5781–5785; (g) H. Zhang, X. Li, L. Zhang, Y. Zhou, X. Ren and M. Liu, *J. Alloys Compd.*, 2018, **749**, 229–235; (h) H. Wu, B. Yan, H. Li, V. Singh, P. Ma, J. Niu and J. Wang, *Inorg. Chem.*, 2018, **57**, 7665–7675.
- 10 (a) M. Shang, C. Li and J. Lin, *Chem. Soc. Rev.*, 2014, **43**, 1372–1386; (b) P. Chen, Q. Li, S. Grindy and N. Holten-Andersen, *J. Am. Chem. Soc.*, 2015, **137**, 11590–11593; (c) M. Mickens, Z. Assefa and D. J. Kumar, *Sol-Gel Sci. Technol.*, 2012, **63**, 153–161; (d) C. Lorbeer and A.-V. Mudring, *J. Phys. Chem. C*, 2013, **117**, 12229–12238; (e) Y. Zhang, G. G. Li, D. L. Geng, M. M. Shang, C. Peng and J. Lin, *Inorg. Chem.*, 2012, **51**, 11655–11664; (f) Z. G. Xia, J. Q. Zhuang, H. K. Liu and L. B. Liao, *J. Phys. D: Appl. Phys.*, 2012, **45**, 015302.
- 11 P. Ma, F. Hu, R. Wan, Y. Huo, D. Zhang, J. Niu and J. Wang, *J. Mater. Chem. C*, 2016, **4**, 5424–5433.
- 12 (a) B. Artetxe, S. Reinoso, F. L. San, L. Lezama, J. M. Gutiérrez-Zorrilla, J. A. García, J. R. Galán-Mascarós, A. Haider, U. Kortz and C. Vicent, *Chem. – Eur. J.*, 2014, **20**, 12144–12156; (b) B. Artetxe, S. Reinoso, F. L. San, J. M. Gutiérrez-Zorrilla, J. A. García, F. Haso, T. Liu and C. Vicent, *Chem. – Eur. J.*, 2015, **21**, 7736–7745.
- 13 (a) J. Zhang, G.-M. Cai, L.-W. Yang, Z.-Y. Ma and Z.-P. Jin, *Inorg. Chem.*, 2017, **56**, 12902–12913; (b) G. M. Cai, N. Yang, H. X. Liu, J. Y. Si and Y. Q. Zhang, *J. Lumin.*, 2017, **187**, 211–220.
- 14 (a) D. Ananias, F. A. A. Paz, D. S. Yufit, L. D. Carlos and J. Rocha, *J. Am. Chem. Soc.*, 2015, **137**, 3051–3058; (b) A. R. Ramya, D. Sharma, S. Natarajan and M. L. P. Reddy, *Inorg. Chem.*, 2012, **51**, 8818–8826; (c) C.-Y. Sun, X.-L. Wang, X. Zhang, C. Qin, P. Li, Z.-M. Su, D.-X. Zhu, G.-G. Shan, K.-Z. Shao, H. Wu and J. Li, *Nat. Commun.*, 2013, **4**, 2717, DOI: 10.1038/ncomms3717.
- 15 C. M. Tourne and G. F. Tourne, *J. Chem. Soc., Dalton Trans.*, 1988, 2411.
- 16 G. M. Sheldrick, *Acta Crystallogr., Sect. C: Struct. Chem.*, 2015, **C71**, 3–8.
- 17 A. L. Spek, *Acta Crystallogr., Sect. C: Struct. Chem.*, 2015, **C71**, 9–18.
- 18 K. Wang, Y. Niu, D. Zhao, Y. Zhao, P. Ma, D. Zhang, J. Wang and J. Niu, *Inorg. Chem.*, 2018, **56**, 14053–14059.